TABLE I. Clinical Findings in Affected Males Previously Reported and Our Patient

Family number: report affected males number (examined number)	1: Gilfillan et al. [2008] 3 (3)	2: Gilfillan et al. [2008] 2 (1)	3: Gilfillan et al. [2008] 3 (3)	4: Gilfillan et al. [2008], Christianson et al. [1999] 16 (4)	5: Schroer et al. [2010] 6 (6)	6: Schroer et al. [2010] 1 (1)	Our patient
Development and behavior							
Profound delay	+	+	+	+	+	+	+
Verbal language absent	+	+	+	+	+	+	+
Easily provoked laughter	+	+	+	+	3/6	−	+
CNS findings							
Epilepsy	+	+	+	+	+	+	+
Ataxia	+	+	+	+	NR	NR	+
Hyperkinetic movements	2/3	−	+	−	2/6	NR	−
Strabismus	+	+	+	+	5/6	+	+
Physical findings							
Microcephaly	+	+	+	3/4	5/6	+	+
Open mouth + drooling	2/3	+	+	NR	4/6	+	+
Swallowing difficulty	2/3	+	1/3	1/4	NR	+	−
Flexed arms	+	NR	1/3	+	3/6	−	−
Electroencephalography							
Epileptiform activity	+	+	+	+	+	+	+
Background activity	10–11 Hz	1.5–3 Hz	4–7 Hz	3–6 Hz to 11–14 Hz	NR	α rhythm	5–6 Hz
Brain MRI/autopsy							
Cerebellar atrophy	1/3	NR	NR	2/4	2/6	+	−
Mutation	p.E287_S288del c.936_941delAAAGTG	p.R500X c.1574C → T	p.V176_201del c.679 +1 delGTAA	p.H203fs c.684_685delAT	p.R500X c.1574C → T	p.Q437X c.1391C → T	p.S147fs c.441delG

+, present with all the patients; −, not present; NR, not recorded.

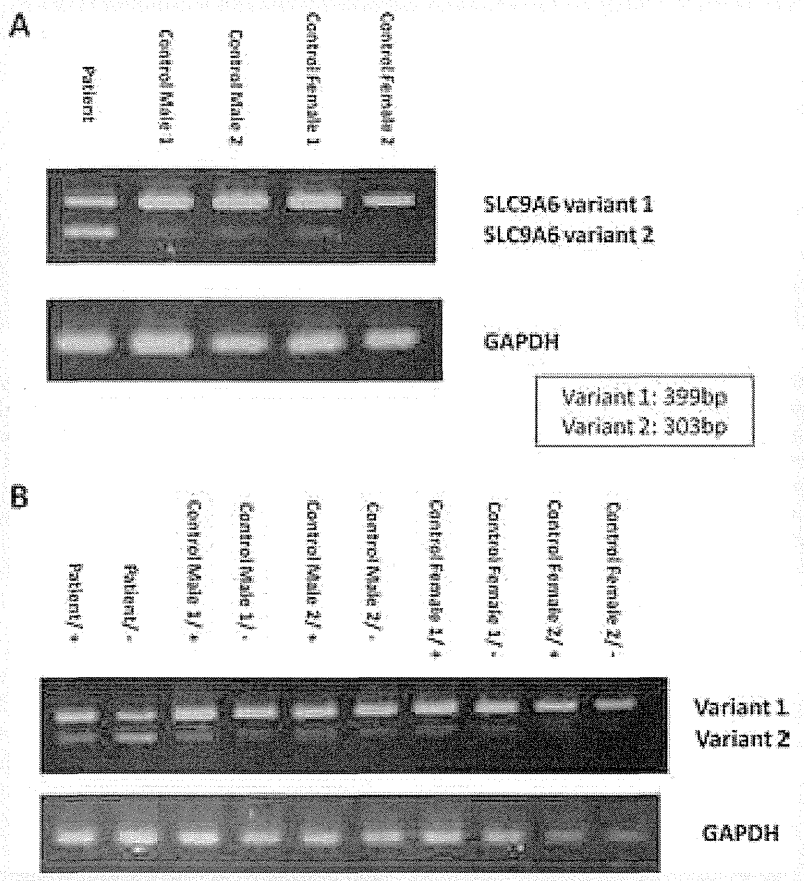

FIG. 3. RT-PCR amplification of the *SLC9A6* gene. A: *SLC9A6* variant 1 mRNA expression was decreased in the patient compared to that in four normal controls. On the other hand, variant 2 expression was increased in the patient compared to that in the controls. B: CHX treatment increases the mutant *SLC9A6* variant 1 mRNA expression, leading to similar expression levels in the patient and four normal controls samples. (+) After CHX treatment, (−) no CHX treatment.

was unchanged (Fig. 4A). The expression level of *SLC9A6* variant 2 increased in all samples after CHX treatment, however the increase was significant only in control samples (Fig. 4B).

Decreased Expression of the NHE6 Protein From Mutant *SLC9A6*

Western blotting was performed to investigate expression of the NHE6 protein in the homogenate of lymphoblastoid cell lines from the patient and his mother. As a result, protein expression of NHE6.1 was not detected in the patient (Fig. 5A,B). The same NHE6.1 was detected in HeLa cells and cells from the patient's mother as well as in the controls. NHE6.0, which was expected to be 10–20 kDa smaller than NHE6.1on SDS–PAGE [Ohgaki et al., 2008], was not detected in any sample (Fig. 5B).

DISCUSSION

In this study we investigated 22 male AS-like patients and 104 male patients with XMR, and identified only one AS-like patient with a *SLC9A6* frameshift mutation. This result further confirms *SLC9A6* is not a major cause of AS-like cases, as reported by Fichou et al. [2009]. Although the number of patients with XMR in this study was small, *SLC9A6* is likely to account for only small proportion of XMR cases.

Patients with *SLC9A6* mutations reported by Gilfillan et al., exhibit cardinal features similar to those of AS including severe developmental delay, mental retardation with absent or minimal use of words, easily provoked laughter, ataxia, epilepsy, hyperkinetic movement, nystagmus, and microcephaly.

Gilfillan et al. also identified possible features of difference between these patients and AS patients, including slow progression of symptoms, thin body, cerebellar atrophy, increased glutamate/

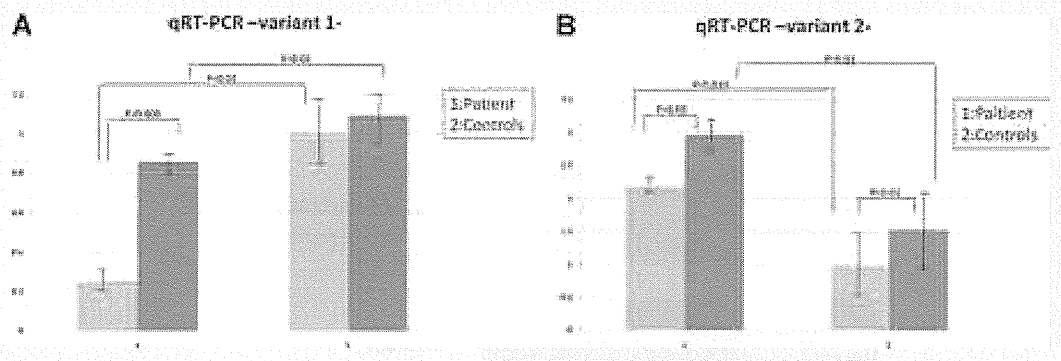

FIG. 4. Real-time quantitative PCR in samples from cell lines from the patient and four normal controls containing two males and two females. The light gray bars indicate the expression levels of *SLC9A6* before CHX treatment, while deep gray bars after CHX treatment. We performed statistical analysis using paired and unpaired Student's *t*-test. Error bars show standard deviation. A: The *SLC9A6* variant 1 was significantly downregulated in samples from the patient while it was not downregulated in samples from four normal controls. After CHX treatment, expression level of the *SLC9A6* variant 1 mRNA in the patient's sample was significantly increased. B: The *SLC9A6* variant 2 in the patient's sample was significantly increased compared to normal controls. Expression level of *SLC9A6* variant 2 increased in all samples after CHX treatment, but a significant increase was only seen in samples from controls.

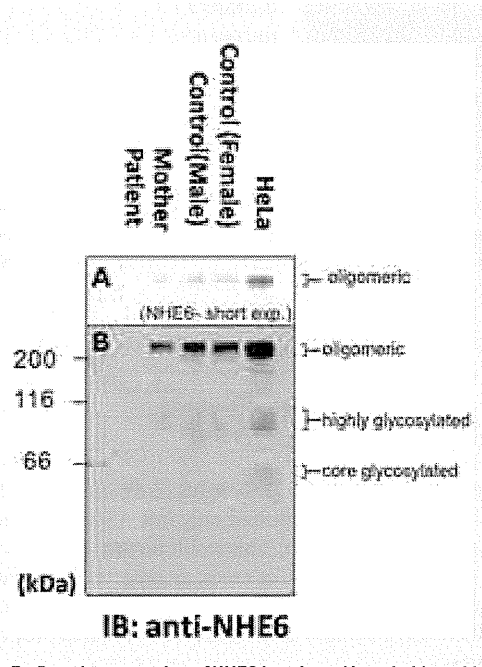

FIG. 5. Protein expression of NHE6 in cultured lymphoblastoid cells and HeLa cells. In the patient, no protein expression of NHE6 isoforms was detected with Western blotting using anti-NHE6 antibody. A: A cropped image taken using a short exposure time demonstrating the oligomeric form of NHE6. Protein size in kDa is shown by numbers on the left of the image. B: A chemiluminescence image of Western blotting taken with a longer exposure time.

glutamic acid peak on MRS, and rapid frequency of 10–14 Hz waves on EEG (Table I). Our patient lost his ability to walk although he did not demonstrate spasticity, demonstrating a slowly progressive clinical course consistent with findings in Gilfillan's report. Indeed, slow progression may be a distinctive clinical feature for patients with *SLC9A6* mutations. One of the families which Gilfillan et al. investigated was previously reported by Christianson et al. [1999], and designated as Christianson syndrome. Schroer et al. reported patients with Christianson syndrome, and they showed that the patients demonstrated an AS-like phenotype. However, while the clinical features of our patient were consistent with those of most patients previously reported by Gilfillan, there were differences including the EEG findings and lack of cerebellar atrophy. Despite this, our patient did meet the diagnostic criteria for AS [Williams et al., 2006]. Therefore, this study further demonstrated that a patient with a *SLC9A6* mutation may resemble patients with AS. Further, this striking similarity between patients with AS and those with *SLC9A6* mutations suggests a possible relationship between the gene function of *UBE3A* and *SLC9A6* in the developing brain.

Our patient's mutation created a frameshift resulting in 7 missense amino acids followed by a stop codon. This mutation was present only in *SLC9A6* transcript variant 1. *SLC9A6* mRNA has two transcript variants caused by alternative splicing in exon 2 (Fig. 1), but the role of each variant has not been clarified. The mutation detected in our patient only affects variant 1 sequence, but the phenotype of the patient was as severe as those in previously reported patients. Therefore, our finding suggests that the NHE6.1 plays an important role in brain function.

Nonsense mediated decay is involved in regulating the expression of alternatively spliced forms containing PTCs [Lareau et al., 2007; Ni et al., 2007]. Since the identified mutation was predicted to result in a PTC, we speculated that NMD could be involved in disease pathogenesis. The result of qRT-PCR showed a significant

decrease in *SLC9A6* variant 1 mRNA expression in the patient sample. This reduction was restored by CHX treatment, while *SLC9A6* variant 1 expression was unaltered by CHX treatment in normal control samples. Expression of *SLC9A6* variant 2 in the patient on the other hand, was significantly increased compared to that in control samples, however it was not influenced by CHX treatment. Therefore, the c.441delG mutation in the patient seems to have modified the alternative splicing pattern, leading to an increase in variant 2 expression. Alternatively, low variant 1 could trigger a regulatory feed back on transcription causing the apparent increase in variant 2 expression. A mutation causing premature protein truncation could alter the splicing pattern and lead to exon skipping, use of alternative splice sites, and intron retention [Hentze and Kulozik, 1999; Mendell and Dietz, 2001]. Our results indicated that the c.441delG mutation caused a PTC altered the splicing pattern, and activated NMD machinery then downregulated *SLC9A6* variant 1 expression.

As protein NHE6.1 was not detected, this indicates an absence of intact NHE6.1. NHE6.0 was also not detected. These findings conclusively indicated that the identified mutation should cause total loss-of-function. Recently, Garbern et al. identified cases with an in-frame deletion of three amino acids, who showed milder dysmorphic features and higher gross motor abilities than those in cases previously reported [Garbern et al., 2010]. Their in-frame deletion should not cause total loss-of-function but create a mildly dysfunctional protein. Therefore, severe phenotypes including severe developmental delay and progressive neurological deterioration may be caused by truncated mutations and less severe phenotypes may be caused by missense or in-frame mutations, and such mild phenotypes are likely missed in patients with mild developmental delay.

Given that the *SLC9A6* variant 2 was upregulated, we speculated that upregulated variant 2 might partially compensate for the absence of NHE6.1. However, we could not establish the upregulation of the NHE6.0 protein, rather it was not detected in the patient's lymphoblastoid cells. NHE6.0 may be unstable compared to NHE6.1. Alternately, NHE6.0 translation may be inhibited. Further investigation is required to definitively answer this question.

NHE6 is found in the membranes of early recycling endosomes and transiently in plasma membranes. Its distribution is regulated by RACK1 [Ohgaki et al., 2008]. Recycling endosomal trafficking is essential for the growth of dendritic spines during LTP in the brain [Park et al., 2006]. The function of the protein product of *UBE3A*, E3 ubiquitin ligase, is also associated with dendritic spine morphology. Mice with a maternal null mutation in *Ube3a* are also reported to have defects in LTP, and manifest motor and behavioral abnormalities [Jiang et al., 1998]. In a recent study, *Ube3a* deficient mice demonstrated dendritic spine dysmorphology [Dindot et al., 2008]. Thus, *UBE3A* and *SLC9A6* could interact in a common pathway involved in dendritic spine development, with a mutation in either leading to an AS-like phenotype.

ACKNOWLEDGMENTS

The authors thank Dr. Tadashi Ariga for critical reading of the manuscript.

REFERENCES

Aznarez I, Zielenski J, Rommens JM, Blencowe BJ, Tsui LC. 2007. Exon skipping through the creation of a putative exonic splicing silencer as a consequence of the cystic fibrosis mutation R533X. J Med Genet 44: 341–346.

Brett CL, Wei Y, Donowitz M, Rao R. 2002. Human Na(+)/H(+) exchanger isoform 6 is found in recycling endosomes of cells, not in mitochondria. Am J Cell Physiol 5:1031–1041.

Carter MS, Doskow J, Morris P, Li S, Nhim RP, Sandstedt S, Wilkinson MF. 1995. A regulatory mechanism that detects premature nonsense codons in T-cell receptor transcripts in vivo is reversed by protein synthesis inhibitors in vitro. J Biol Chem 270:28995–29003.

Christianson AL, Stevenson RE, van der Meyden CH, Pelser J, Theron FW, van Rensburg PL, Chandler M, Schwartz CE. 1999. X linked severe mental retardation, craniofacial dysmorphology, epilepsy, ophthalmoplegia, and cerebellar atrophy in a large South African kindred in localized to Xq24–q27. J Med Genet 36:759–766.

Dindot SV, Antalffy BA, Bhattacharjee MB, Beaudet AL. 2008. The Angelman syndrome ubiquitin ligase localizes to the synapse and nucleus, and maternal deficiency results in abnormal dendritic spine morphology. Hum Mol Genet 17:111–118.

Fichou Y, Bahi-Buisson N, Nectoux J, Chelly J, Heron D, Cuisset L, Bienvenu T. 2009. Mutation in the *SLC9A6* gene is not a frequent cause of sporadic Angelman-like syndrome. Eur J Hum Genet 17:1378–1380.

Garbern JY, Neumann M, Trojanowski JQ, Lee VM, Feldman G, Norris JW, Friez MJ, Schwartz CE, Stevenson R, Sima AA. 2010. A mutation affecting the sodium/proton exchanger, *SLC9A6*, causes mental retardation with tau deposition. Brain 133:1391–1402.

Gilfillan GD, Selmer KK, Roxrud I, Smith R, Kyllerman M, Eiklid K, Kroken M, Mattingsdal M, Egeland T, Stenmark H, Sjoholm H, Server A, Samuelsson L, Christianson A, Tarpey P, Whibley A, Stratton MR, Futreal A, Teague J, Edkins S, Gecz J, Turner G, Raymond FL, Schwartz C, Stevenson RE, Undlien DE, Stromme P. 2008. *SLC9A6* mutations cause X-linked mental retardation, microcephaly, epilepsy, and ataxia, a phenotype mimicking Angelman Syndrome. Am J Hum Genet 82: 1003–1010.

Hentze MW, Kulozik AE. 1999. A perfect message: RNA surveillance and nonsense-mediated decay. Cell 96:307–310.

Jiang YH, Armstrong D, Albrecht U, Atkins CM, Noebels JI, Eichele G, Sweatt JD, Beaudet AL. 1998. Mutation of the Angelman ubiquitin ligase in mice causes increased cytoplasmic p53 and deficits of contextual learning and long-term potentiation. Neuron 21:799–811.

Lareau LF, Inada M, Green RE, Wengrod JC, Brenner SE. 2007. Unproductive splicing of SR genes associated with highly conserved and ultraconserved DNA elements. Nature 446:926–929.

Mendell JT, Dietz HC. 2001. When the message goes awry: Disease-producing mutations that influence mRNA content and performance. Cell 107:411–414.

Nakamura N, Tanaka S, Teko Y, Mitsui K, Kanazawa H. 2005. Four Na^+/H^+ exchanger isoforms are distributed to Golgi and post-Golgi compartments and are involved in organelle pH regulation. J Biol Chem 280:1561–1572.

Ni JZ, Grate L, Donohue JP, Preston C, Nobida N, O'Brien G, Shiue L, Clark TA, Blume JE, Ares M, Jr. 2007. Ultraconserved elements are associated with homeostatic control of splicing regulators by alternative splicing and nonsense-mediated decay. Genes Dev 21:708–718.

Ohgaki R, Fukura N, Matsushita M, Mitsui K, Kanazawa H. 2008. Cell surface levels of organellar Na^+/H^+ exchanger isoform 6 are regulated by interaction with RACK1. J Biol Chem 283:4417–4429.

Park M, Salgado JM, Ostroff L, Helton TD, Robinson CG, Harris KM, Ehlers MD. 2006. Plasticity-induced growth of dendritic spines by exocytic trafficking from recycling endosomes. Neuron 52:817–830.

Roxrud I, Raiborga C, Gilfillan GD, Strømmed P, Stenmark H. 2009. Dual degradation mechanisms ensure disposal of NHE6 mutant protein associated with neurological disease. Exp Cell Res 135:3014–3027.

Saitoh S, Wada T, Okajima M, Takano K, Sudo A, Niikawa N. 2005. Uniparental disomy and imprinting defects in Japanese patients with Angelman syndrome. Brain Dev 27:389–391.

Schroer RJ, Holden KR, Tarpey PS, Matheus MG, Griesemer DA, Friez MJ, Fan JZ, Simensen RJ, Stromme P, Stevenson RE, Stratton MR, Schwartz CE. 2010. Natural history of Christianson syndrome. Am J Med Genet Part A 152A:2775–2783.

Takano K, Nakagawa E, Inoue K, Kamada F, Kure S, Goto Y, Japanese Mental Retardation Consortium. 2008. A loss-of-function mutation in the FTSJ1 gene causes nonsyndromic X-linked mental retardation in a Japanese family. Am J Med Genet Part B 147B:479–484.

Williams CA, Beaudet AL, Clayton-Smith J, Knoll JH, Kyllerman M, Laan LA, Magenis RE, Moncla A, Schinzel AA, Summers JA, Wagstaff J. 2006. Angelman Syndrome 2005: Updated consensus for diagnostic criteria. Am J Med Genet Part A 140A:413–418.

RESEARCH LETTER

AMERICAN JOURNAL OF medical genetics PART A

Tissue-Limited Ring Chromosome 18 Mosaicism as a Cause of Pitt–Hopkins Syndrome

Toshiki Takenouchi,[1] Tatsuhiko Yagihashi,[1,2] Hiroyuki Tsuchiya,[3] Chiharu Torii,[4] Kumiko Hayashi,[5] Rika Kosaki,[6] Shinji Saitoh,[7] Takao Takahashi,[1] and Kenjiro Kosaki[1,4]*

[1]Department of Pediatrics, Keio University School of Medicine, Tokyo, Japan

[2]Center for Clinical Research, Keio University School of Medicine, Tokyo, Japan

[3]Department of Pediatrics, Tachikawa Kyosai Hospital, Tokyo, Japan

[4]Center for Medical Genetics, Keio University School of Medicine, Tokyo, Japan

[5]Mitsubishi Chemical Medience Corporation, Tokyo, Japan

[6]Division of Medical Genetics, National Center for Child Health and Development, Tokyo, Japan

[7]Department of Pediatrics and Neonatology, Nagoya City University Graduate School of Medical Sciences, Nagoya, Japan

Manuscript Received: 25 August 2011; Manuscript Accepted: 31 December 2011

TO THE EDITOR:

We wish to congratulate the authors on their detailed review of Pitt–Hopkins syndrome (PTHS, [OMIM 610954]) published in a recent issue of this journal [Marangi et al., 2011]. PTHS represents a rare disorder with characteristic facial gestalt, episodic hyperventilation, and severe developmental delay with absent speech [Pitt and Hopkins, 1978]. Haploinsufficiency of transcription factor 4 (TCF4) gene at chromosome 18q21.2 is responsible for PTHS [Brockschmidt et al., 2007; Zweier et al., 2007]. The comprehensive review by Marangi et al. illustrated that TCF4 point mutations, balanced translocations spanning the TCF4 locus, and even very large 18q deletions can result in the distinctive PTHS phenotype as long as the TCF4 locus is deleted. Here, we wish to demonstrate that ring (18) mosaicism represents yet another mechanism leading to the classic PTHS phenotype.

The propositus was born to unrelated Japanese parents. Her family history was non-contributory, with one older sister who is developing normally. The propositus was born at 40 and 1/7 weeks gestation via normal spontaneous vaginal delivery. Her birth weight was 2,805 g, and her head circumference was 32.3 cm. Soon after birth, she exhibited frequent episodes of projective vomiting caused by severe gastroesophageal reflux. Subsequently, she developed recurrent aspiration pneumonia requiring multiple hospital admissions. A magnetic resonance imaging of the brain at the age of 23 months revealed "delayed myelination" consistent with an age of 15 months but no other major structural abnormalities. A G-band chromosome analysis performed at that time was reportedly normal. She was first presented to us at the age of 3 years because of severe developmental delays. Her weight was 9.8 kg (−2.1 SD), height 83.8 cm (−2.1 SD), and head circumference 44.4 cm (−3.2 SD). Upon examination, she had a happy disposition with unexpected laughing, clapping of her hands and absent speech, microcephaly, global hypotonia, scoliosis, a short neck and syndactyly, and bilateral single palmar creases. Her finger pads were not prominent. She had characteristic facial features, that is, midfacial hypoplasia, a short philtrum, separated incisors, fleshy ears, downward slanting eyes, a pointed chin, macroglossia, and a prominent lower lip (Fig. 1). There was no apparent brachycephaly (Fig. 1). The serum IgA level was within the normal range, that is, 95 mg/dl [age reference 60–354 mg/dl]. She started to have generalized seizures at the age of 3 years. She is currently 11 years old and is unable to sit without support or to communicate verbally. She has been severely constipated requiring a daily enema. She exhibits episodic apnea-hyperpnea, often provoked by emotional excitement.

A FISH analysis using a BAC probe spanning the TCF4 locus (RP11-1079G18) was performed using a buccal swab specimen, and a mosaic deletion in 97.7% of the cells was revealed (Fig. 2a). An extensive chromosomal G-band analysis of a peripheral blood sample showed 5 ring (18) cells out of the 110 cells that were studied, yielding an average prevalence of one abnormal copy in 22 cells (Fig. 2b). An array comparative genomic hybridization (CGH)

How to Cite this Article:
Takenouchi T, Yagihashi T, Tsuchiya H, Torii C, Hayashi K, Kosaki R, Takahashi T, Kosaki K. 2012. Tissue-limited ring chromosome 18 mosaicism as a cause of Pitt–Hopkins syndrome.
Am J Med Genet Part A 158A:2621–2623.

*Correspondence to:
Kenjiro Kosaki, M.D., Center for Medical Genetics, Keio University School of Medicine, 35 Shinanomachi, Shinjuku, Tokyo 1608582, Japan.
E-mail: kkosaki@z3.keio.jp

Article first published online in Wiley Online Library (wileyonlinelibrary.com): 10 August 2012
DOI 10.1002/ajmg.a.35230

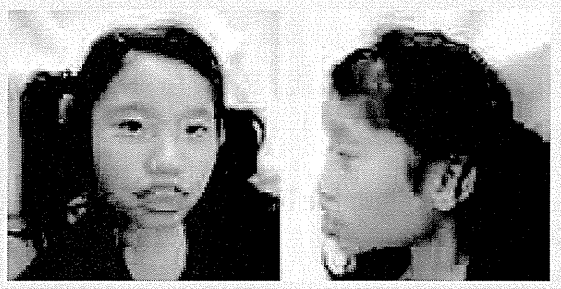

FIG. 1. Facial appearance of the propositus. Note midfacial hypoplasia, a short philtrum, separated incisors, fleshy ears, downward slanting eyes, a pointed chin, macroglossia, and a prominent lower lip.

analysis of her peripheral blood that was performed concurrently with the FISH analysis revealed a 29.12-Mb deletion from position 46,962,563 to 76,083,258 in 18q21.2-q23 and a 1.5-Mb deletion from position 108,560 to 1,617,028 in 18p11.32. The mosaic ratio estimated from an array CGH analysis was 26% according to the method described by Cheung et al. [2007].

The patient reported herein suggests that a ring (18) mosaicism can cause PTHS. A mosaic ring chromosome has not been recognized as a cause of PTHS, although there have been two PTHS patients due to mosaic deletion of TCF4 [Giurgea et al., 2008; Stavropoulos et al., 2010]. It was difficult to ascertain whether PTHS has been overlooked in patients with ring (18) mosaicism, since cytogenetic confirmation of TCF4 involvement has never performed in reported patients with ring (18) mosaicism [Lo-Castro et al., 2011].

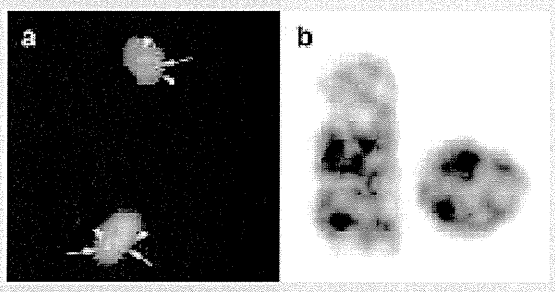

FIG. 2. Cytogenetic analyses of the propositus. a: A interphase FISH analysis of buccal swab specimen using TCF 4 probe (arrows, red) and CEP 18 probe (arrowheads, green) demonstrated 87 cells with one TCF4 probe (top) and two cells with two TCF4 probes (bottom) out of 89 cells that were studied. b: A G-band analysis of a peripheral blood sample revealed presence of ring chromosome 18 (right) in addition to normal chromosome 18 (left), consistent with ring (18) mosaicism.

In retrospect, reaching a correct diagnosis in the propositus was not a straightforward process: a pointed chin in the presence of autism, epilepsy, and a happy disposition with unexpected laughing was suggestive of Angelman syndrome [MIM 105830], whereas hand clapping in the presence of autism and epilepsy was reminiscent of Rett syndrome [MIM 312750], especially in females. Indeed, we had to perform a round of methylation studies and a UBE3A mutation analysis for Angelman syndrome as well as MECP2 mutation analysis before reaching a correct diagnosis. Because PTHS is gradually gaining recognition as differential diagnosis of Angelman syndrome and Rett syndrome among pediatric neurologists, we did perform a FISH for TCF4 on peripheral blood cells, but the test was interpreted as negative apparently because of the extremely low level of mosaicism of the ring (18). Her diagnosis would have been easily missed without performing a FISH using a buccal mucosa sample or an array CGH.

Indeed, the large discrepancy in the level of mosaicism in two aspects of the propositus hindered the diagnosis: first, there was a discrepancy between the mosaic ratio in the peripheral blood obtained from a G-band analysis (5/110) and that estimated from an array CGH analysis (26%). This discrepancy reflects the preferential selection of normal cells (46, XX cells) during the PHA stimulation of T cells required in the G-banding analysis. The array CGH analysis, which does not depend on the PHA stimulation process, is not subject to such an artifactual bias in the assessment of the mosaic rate [Ballif et al., 2006]. Not unexpectedly, in retrospect, the initial G-band analysis failed to detect the presence of cells with ring (18) chromosomes. Second, there was a discrepancy between the mosaic ratio in the peripheral blood evaluated using the array CGH analysis and that obtained from an interphase FISH study using the buccal smear. Since buccal smear FISH is not subject to the selection bias discussed above, the difference in the mosaic rate likely reflects a true difference in the level of mosaicism among tissues (i.e., peripheral blood vs. buccal cells). It is not clear whether the high percentage of abnormal cells in the buccal smear represents the situation in her central nervous system. Given her profound neurological disability, we suspect that her brain tissue may contain a very high percentage of abnormal cells. The situation is quite comparable to Pallister–Killian syndrome (tetrasomy 12p mosaicism), in which a diagnosis is dependent on a FISH study of non-blood tissues [Manasse et al., 2000] or an array CGH study of the blood [Theisen et al., 2009].

Clearly, the haploinsufficiency of deleted genes on chromosome 18q other than TCF4 has contributed to the phenotype of the propositus. The propositus exhibited macroglossia and delayed myelination. Macroglossia has been described in patients with Beckwith–Wiedemann like phenotype and 18q deletion [Brewer et al., 1998; Lirussi et al., 2007]. However, the propositus did not have other features of Beckwith–Wiedemann syndrome, such as overgrowth. The initial brain MRI of the propositus reported delayed myelination, which could be attributable to the deletion of myelin basic protein (MBP, OMIM #159430) located in 18q23 [Popko et al., 1987]. Although severe mental retardation with autistic features can be seen both in 18q deletion syndrome and in PTHS, episodic hyperventilation observed in the propositus is a distinctive feature of PTHS [Ouvrier, 2008]. On the other hand,

some commonly observed features of PTHS were not apparent. The propositus did not have characteristic facial features such as a pointed nasal tip, flaring nostrils, or brachycephaly, which are known features of PTHS [Zweier et al., 2007]. Moreover, Lehalle et al. [2011] reported that several individuals with PTHS have prominent finger pads, which were not apparent in the propositus. The absence of these features might be a consequence of the haploinsufficiency of genes other than TCF4.

In summary, an extensive and thorough investigation of the TCF4 locus, including that on a mosaic ring (18), should be performed in patients with a high clinical suspicion of PTHS.

REFERENCES

Ballif BC, Rorem EA, Sundin K, Lincicum M, Gaskin S, Coppinger J, Kashork CD, Shaffer LG, Bejjani BA. 2006. Detection of low-level mosaicism by array CGH in routine diagnostic specimens. Am J Med Genet Part A 140A:2757–2767.

Brewer CM, Lam WW, Hayward C, Grace E, Maher ER, FitzPatrick DR. 1998. Beckwith-Wiedemann syndrome in a child with chromosome 18q deletion. J Med Genet 35:162–164.

Brockschmidt A, Todt U, Ryu S, Hoischen A, Landwehr C, Birnbaum S, Frenck W, Radlwimmer B, Lichter P, Engels H, et al. 2007. Severe mental retardation with breathing abnormalities (Pitt-Hopkins syndrome) is caused by haploinsufficiency of the neuronal bHLH transcription factor TCF4. Hum Mol Genet 16:1488–1494.

Cheung SW, Shaw CA, Scott DA, Patel A, Sahoo T, Bacino CA, Pursley A, Li J, Erickson R, Gropman AL, et al. 2007. Microarray-based CGH detects chromosomal mosaicism not revealed by conventional cytogenetics. Am J Med Genet Part A 143A:1679–1686.

Giurgea I, Missirian C, Cacciagli P, Whalen S, Fredriksen T, Gaillon T, Rankin J, Mathieu-Dramard M, Morin G, Martin-Coignard D, et al. 2008. TCF4 deletions in Pitt-Hopkins Syndrome. Hum Mutat 29: E242–E251.

Lehalle D, Williams C, Siu VM, Clayton-Smith J. 2011. Fetal pads as a clue to the diagnosis of Pitt-Hopkins syndrome. Am J Med Genet Part A 155A:1685–1689.

Lirussi F, Jonard L, Gaston V, Sanlaville D, Kooy RF, Winnepenninckx B, Maher ER, Fitzpatrick DR, Gicquel C, Portnoi MF, et al. 2007. Beckwith-Wiedemann-like macroglossia and 18q23 haploinsufficiency. Am J Med Genet Part A 143A:2796–2803.

Lo-Castro A, El-Malhany N, Galasso C, Verrotti A, Nardone AM, Postorivo D, Palmieri C, Curatolo P. 2011. De novo mosaic ring chromosome 18 in a child with mental retardation, epilepsy and immunological problems. Eur J Med Genet 54:329–332.

Manasse BF, Lekgate N, Pfaffenzeller WM, de Ravel TJ. 2000. The Pallister-Killian syndrome is reliably diagnosed by FISH on buccal mucosa. Clin Dysmorphol 9:163–165.

Marangi G, Ricciardi S, Orteschi D, Lattante S, Murdolo M, Dallapiccola B, Biscione C, Lecce R, Chiurazzi P, Romano C, et al. 2011. The Pitt-Hopkins syndrome: Report of 16 new patients and clinical diagnostic criteria. Am J Med Genet Part A 155A:1536–1545.

Ouvrier R. 2008. Hyperventilation and the Pitt-Hopkins syndrome. Dev Med Child Neurol 50:481.

Pitt D, Hopkins I. 1978. A syndrome of mental retardation, wide mouth and intermittent overbreathing. Aust Paediatr J 14:182–184.

Popko B, Puckett C, Lai E, Shine HD, Readhead C, Takahashi N, Hunt SW III, Sidman RL, Hood L. 1987. Myelin deficient mice: Expression of myelin basic protein and generation of mice with varying levels of myelin. Cell 48:713–721.

Stavropoulos DJ, MacGregor DL, Yoon G. 2010. Mosaic microdeletion 18q21 as a cause of mental retardation. Eur J Med Genet 53:396–399.

Theisen A, Rosenfeld JA, Farrell SA, Harris CJ, Wetzel HH, Torchia BA, Bejjani BA, Ballif BC, Shaffer LG. 2009. aCGH detects partial tetrasomy of 12p in blood from Pallister-Killian syndrome cases without invasive skin biopsy. Am J Med Genet Part A 149A:914–918.

Zweier C, Peippo MM, Hoyer J, Sousa S, Bottani A, Clayton-Smith J, Reardon W, Saraiva J, Cabral A, Gohring I, et al. 2007. Haploinsufficiency of TCF4 causes syndromal mental retardation with intermittent hyperventilation (Pitt-Hopkins syndrome). Am J Hum Genet 80:994–1001.

Research Article

Developmental Dynamics
DOI 10.1002/dvdy.24099

Soluble form of FGFR2 with S252W partially prevents craniosynostosis of the Apert mouse model

Jumpei Morita [1,2], Masataka Nakamura [2], Yukiho Kobayashi [1,3], Chu-Xia Deng [4], Noriko Funato [2], Keiji Moriyama [1,3,*]

[1]Maxillofacial Orthognathics, Department of Maxillofacial Reconstruction and Function, Graduate School of Medical and Dental Sciences, Tokyo Medical and Dental University, Tokyo 113-8549, Japan

[2]Human Gene Sciences Center, Tokyo Medical and Dental University, Tokyo 113-8510, Japan

[3]Hard Tissue Genome Research Center, Tokyo Medical and Dental University, Tokyo 113-8549, Japan

[4]Genetics of Development and Disease Branch, National Institute of Diabetes, Digestive and Kidney Diseases, US National Institutes of Health, 10 Center Drive, Bethesda, Maryland 20892, USA

*Corresponding author. Maxillofacial Orthognathics, Department of Maxillofacial Reconstruction and Function, Graduate School of Medical and Dental Sciences, Tokyo Medical and Dental University, 1-5-45 Yushima, Bunkyo-ku, Tokyo 113-8549, Japan. Phone number: +81 3 5803 5534; E-mail: k-moriyama.mort@tmd.ac.jp

Running Title: Soluble FGFR2 prevents Apert syndrome

Key words: craniofacial; Apert syndrome; osteogenesis; pharmacodynamics

Received: Jul 11, 2013; Revised: Nov 12, 2013; Accepted: Nov 17, 2013

Bullet points: We generated an $Fgfr2^{+/S252W}$ Apert mouse model expressing a soluble form of $FGFR2^{S252W}$.

The soluble form of $FGFR2^{S252W}$ partially rescued Apert syndrome-like phenotypes *in vivo.*

$Fgfr2^{+/S252W}$ mice exhibited ectopic bone and thickened cartilage formation in interfrontal sutures.

Grant Sponsor: Grants-in-Aid for Scientific Research from the Japanese Society for the Promotion of Science; Grant numbers: 18209060, 23390471

Abstract

Background: Apert syndrome (AS) is characterized by craniosynostosis, midfacial hypoplasia, and bony syndactyly. It is an autosomal dominantly inherited disease caused by point mutations (S252W or P253R) in fibroblast growth factor receptor (FGFR) 2. These mutations cause activation of FGFR2 depending on ligand binding. Recently, an AS mouse model, *Fgfr2*$^{+/S252W}$, showed phenotypes similar to those of AS patients. We previously reported that the soluble form of FGFR2^{S252W} (sFGFR2IIIc^{S252W}) efficiently inhibits enhanced osteoblastic differentiation caused by FGFR2 activation in AS *in vitro*, presumably because FGFs binding to FGFRs is interrupted. In this study, we developed *Fgfr2*$^{+/S252W}$ (Ap) mice expressing the sFGFR2IIIc^{S252W} protein, and we investigated the effects of sFGFR2IIIc^{S252W} on AS-like phenotypes. Results: In Ap mice, the coronal suture (CS) was fused prematurely at P1. In addition, the mice exhibited a widened interfrontal suture (IFS) with ectopic bone and thickened cartilage formation. In *Fgfr2*$^{+/S252W}$ *sFGFR2IIIc*^{S252W} (Ap/Sol) mice, the CS was similar to that of wild-type mice. Ap/Sol mice did not show any ectopic bone or cartilage formation in the IFS, but showed a wider IFS than that of the wild-type mice. Conclusions: sFGFR2IIIc^{S252W} may partially prevent craniosynostosis in the Apert mouse model by affecting the CS and IFS *in vivo*.

Introduction

Apert syndrome (AS) (OMIM: 101200) is an autosomal dominantly inherited syndrome characterized by craniosynostosis, midfacial hypoplasia, and symmetric bony syndactyly of the hands and feet. It occurs in approximately 1/65,000 births and accounts for 4.5% of all craniosynostosis (Cohen et al., 1992). AS is caused by one of two missense mutations of the fibroblast growth factor receptor (FGFR) 2 gene involving the following amino acid substitutions: S252W or P253R (Wilkie et al., 1995; Oldridge et al., 1997; Oldridge et al., 1999), resulting in gain-of-function of fibroblast growth factor (FGF) signaling (Anderson et al., 1998; Ibrahimi et al., 2001).

FGFRs constitute a family of four membrane-spanning tyrosine kinases, and 18 FGF ligands have been identified (Powers et al., 2000; Ornitz and Itoh, 2001; Coumoul and Deng, 2003). FGFR signaling induces the proliferation, migration, differentiation, and survival of many cell types (Ornitz & Itoh, 2001; Eswarakumar et al., 2005). FGFRs contain a hydrophobic leader sequence, three immunoglobulin (Ig)-like domains, an acidic box, transmembrane region, and a divided tyrosine kinase domain. The IgIII domains of FGFR1–3 are encoded for by exons 7–9. Inclusion of exons 8 and 9 is mutually exclusive, producing the IIIb and IIIc splice isoforms. FGFR2IIIb is located in the epithelium and mainly binds to FGF7 and 10, whereas FGFR2IIIc is present in the mesenchyme and has a high affinity for FGF2, 4, 6, 8, and 9. AS mutations cause loss of ligand specificity of FGFR2 isoforms (Yu et al., 2000).

Recently, two independent mouse models of *Fgfr2*$^{+/S252W}$ (Chen et al., 2003; Wang et al., 2005) and *Fgfr2*$^{+/P253R}$ (Yin et al., 2008; Wang et al., 2010) have been established. Similar to AS patients, both models exhibit premature coronal suture (CS) fusion, midfacial

hypoplasia, and a domed skull. Furthermore, Wang et al. have reported enhanced chondrogenic markers and ectopic cartilage formation in the *Fgfr2*$^{+/S252W}$ mice at sagittal sutures, while the interfrontal sutures (IFSs) showed defects without any cartilage formation (Wang et al., 2005). They proposed that the incorrect migration or localization of neural crest cells caused this ectopic cartilage formation given the difference in tissue origin between the sagittal suture and IFS (Wang et al., 2005). In humans, infants with AS frequently show bone defects in the calvarial midline with a varying degree of heterotopic bone formation between the osteogenic fronts (Cohen & Kreiborg, 1996). Some reports have described the effects of the AS mutations on downstream signaling pathways *in vivo* (Shukla et al., 2007; Yin et al., 2008; Holmes et al., 2009; Wang et al., 2010). These mouse models are used to evaluate novel targets and strategies for treatment of AS. The MEK1 inhibitor PD98059 was shown to reduce CS fusion in calvarial explants from *Fgfr2*$^{+/P253R}$ mice (Yin et al., 2008). Both pre- and post-natal administration of the MEK1/2 inhibitor U0126 inhibited AS-like phenotypes in *Fgfr2*$^{+/S252W}$ male mice, as did gene therapy to express a short hairpin RNA against the *Fgfr2*^{S252W} allele (Shukla et al., 2007). However, synostosis resumed after withdrawal of the chemical inhibitor, which reflects the postoperative re-synostosis phenomenon frequently observed in syndromic craniosynostosis patients. Inhibitors of other pathways that promote osteoblastic differentiation may provide alternatives for direct inhibition of FGF signaling (Holmes, 2012), but they have not been evaluated in an AS mouse model.

Our previous study demonstrated that a soluble form of the Apert mutant FGFR2 (sFGFR2IIIc^{S252W}), which lacks the transmembrane and cytoplasmic domains, acted as a decoy receptor by competing for ligand binding with FGFRs. This mutant inhibited enhanced osteoblastic differentiation in the MG63 osteosarcoma cell line transfected with

FGFR2IIIc^{S252W} (Tanimoto et al., 2004). Furthermore, calvarial osteoblasts derived from *FGFR2IIIc*^{S252W} transgenic mice proliferated and differentiated via highly activated MEK, ERK, and p38 pathways, whereas these pathways were suppressed in calvarial osteoblasts expressing sFGFR2IIIc^{S252W} (Suzuki et al., 2012). To evaluate the inhibitory effect of FGFR2IIIc^{S252W} *in vivo*, we examined the effects of sFGFR2IIIc^{S252W} on the *Fgfr2*$^{+/S252W}$ background in this study.

Results

Generation of mutant mice

To examine the therapeutic effects of sFGFR2IIIc^{S252W} on the Apert mouse model, we generated triple mutant mice with *EIIa-Cre*, *Fgfr2*$^{+/Neo\text{-}S252W}$, and *sFGFR2IIIc*^{S252W}. Mating of *Fgfr2*$^{+/Neo\text{-}S252W}$ with *EIIa-Cre sFGFR2IIIc*^{S252W} mice produced various genotypes such as wild-type, *EIIa-Cre*, *sFGFR2IIIc*^{S252W}, *Fgfr2*$^{+/Neo\text{-}S252W}$, *EIIa-Cre Fgfr2*$^{+/Neo\text{-}S252W}$ (Ap), *sFGFR2IIIc*^{S252W} *Fgfr2*$^{+/Neo\text{-}S252W}$, *EIIa-Cre sFGFR2IIIc*^{S252W}, and *EIIa-Cre sFGFR2IIIc*^{S252W} *Fgfr2*$^{+/Neo\text{-}S252W}$ (Ap/Sol) (Table 1). Genotypic analysis of 242 offspring showed that the genotype distribution was different from the theoretical values. The frequencies of *Fgfr2*$^{+/Neo\text{-}S252W}$, *EIIa-Cre sFGFR2IIIc*^{S252W}, and Ap/Sol mice were lower than expected, while higher values were observed for *EIIa-Cre* and *sFGFR2IIIc*^{S252W} mice.

A previous study has indicated that transcript levels of the exogenous *sFGFR2IIIc*^{S252W} gene in calvarial tissue were marginal (Suzuki et al., 2012). Therefore, we measured the protein levels of sFGFR2IIIc^{S252W} in the blood of *sFGFR2IIIc*^{S252W} mice because sFGFR2IIIc^{S252W} could be present in blood as a result of its transcription in tissues other than the calvaria. Western blot analysis demonstrated that FLAG-tagged

sFGFR2IIIc^{S252W} proteins with molecular masses of about 60 kDa and 35 kDa were present in the serum of sFGFR2IIIc^{S252W} mice (Fig. 1C). Wild-type mice did not show expression of these proteins. The 60-kDa protein was likely native sFGFR2IIIc^{S252W}-3xFLAG, while the 35-kDa protein might have been a degradation product of full-length sFGFR2IIIc^{S252W}-3xFLAG *in vivo*.

Macroscopic examination of Fgfr2$^{+/S252W}$ and sFGFR2IIIc^{S252W} Fgfr2$^{+/S252W}$ mice

General inspection of the appearance of the whole body indicated that Ap mice at P1 were apparently smaller than wild-type mice as reported previously (Fig. 2A) (Chen et al., 2003; Shukla et al., 2007). Ap/Sol mice had a body size between that of Ap and wild-type mice (Fig. 2A). Measurement of body weight supported the observations based on appearance. Body weights of Ap/Sol mice were higher than those of Ap mice but lower than those of wild-type mice, although the differences were not statistically significant (Fig. 2B).

Rescue of the Apert mouse model phenotype by sFGFR2IIIc^{S252W}

To examine the therapeutic effects of sFGFR2IIIc^{S252W} on AS-like phenotypes, triple mutant (Ap/Sol) mice were subjected to micro-CT analysis for morphological characterization and bone mineral density (BMD) analysis, then compared with Ap and wild-type mice. Ap mice had the same BMD at the equivalent site of the coronal suture as the parietal and frontal bones, presumably indicating premature fusing of the CS (white arrowheads in Fig. 3Ab, e), as shown previously in human AS. A wide bony defect at the IFS was also observed in Ap mice at P1 (white arrow in Fig. 3Ah) and P8 (red arrowheads in Fig. 3Bb). Introduction of

sFGFR2IIIc^{S252W} to Ap mice altered the CS phenotypes to those that were between the phenotypes of the wild-type and Ap mice. In addition, the IFS of Ap/Sol mice at P1 was narrower, and the width was close to that of wild-type mice (white arrow in Fig. 3Ai). At P8, there was little difference between Ap/Sol and wild-type mice (Fig. 3Bc). BMD of the parietal bone and IFS width were estimated based on micro-CT data. No significant difference was observed among wild-type, Ap, and Ap/Sol mice in BMD (Fig. 3C). IFS widths in Ap/Sol mice were close to those in wild-type mice, but statistically different from those in Ap mice (Fig. 3D).

In Ap mice (at P1), histological analysis demonstrated that the osteogenic fronts in the CS were irregular and fused prematurely (arrow in Fig. 4Ab). Ap/Sol mice exhibited a patent osteogenic front in the CS very close to that of the wild-type phenotype (Fig. 4Ac). Interestingly, ectopic bone formation and greatly thickened calvarial cartilage in wide IFS were obvious in Ap mice (arrowheads in Fig. 4Bb, e, h), while heterotopic skeletal tissues were not observed in Ap/Sol mice (Fig. 4Bc, f, i). The incidences of the AS-like phenotypes are summarized in Table 2. The frequencies of CS irregularity and IFS with ectopic bones of Ap/Sol mice were significantly different compared to those of Ap mice, while there were no significant differences between those of wild-type and Ap/Sol mice. The frequencies of widened IFS of Ap/Sol mice were lower than those of Ap mice but higher than those of wild-type mice, although the differences were not statistically significant.

Discussion

We investigated the effects of sFGFR2IIIc^{S252W} on Ap mice. Our results showed, for the first time, that sFGFR2IIIc^{S252W} partially rescued the AS-like phenotypes, including low body weight, CS synostosis, ectopic bone formation, thickened cartilage, and widened IFSs *in vivo*. Previous studies have described these syndrome phenotypes in Ap mice, with the exception of ectopic bone formation and thickened cartilage in IFSs, which were observed in this study (Chen et al., 2003; Wang et al., 2005; Shukla et al., 2007; Holmes et al., 2009).

Ectopic cartilage formation in IFSs, which are derived from neural crest cells (Jiang et al., 2002), presumably results from aberrant FGF signaling in pre-migratory neural crest cells at an early embryonic stage as previously indicated *in vitro* (Petiot et al., 2002). This mechanism may support our observation of thickened cartilage formation in the IFS of Ap mice. Interestingly, we observed for the first time ectopic bone formation in the wide IFS of Ap mice, which has been demonstrated in human AS patients (Kreiborg & Cohen, 1990; Cohen & Kreiborg, 1996).

We hypothesize that the reversal of AS-like phenotypes is, at least in part, attributable to repression of aberrantly enhanced FGF signaling in Ap mice by the dominant negative effects of sFGFR2IIIc^{S252W}, which acts as a decoy receptor *in vivo*. This notion is supported by our observations and previous studies by others. We have observed that sFGFR2IIIc^{S252W} can bind a broad range of ligands and dimerize with normal membrane FGFR2 (Yokota et al., unpublished data); sFGFR2IIIc^{S252W} also inhibited aberrant mineralization of MG63 cells overexpressing FGFR2^{S252W} (Tanimoto et al., 2004). In addition, we observed that sFGFR2IIIc^{S252W} repressed the enhanced signaling of the

MEK, ERK, and p38 pathways in osteoblasts expressing FGFR2^{S252W} (Suzuki et al., 2012). A previous study has shown the recovery of AS-like phenotypes in Ap mice by administration of an inhibitor U0126 for the MEK-ERK pathway, which is downstream of FGFR (Shukla et al., 2007). Collectively, Ap/Sol mice appeared to have partial recovery of the AS-like phenotypes. The MEK-ERK pathway, which is inhibited by U0126, is involved in the pathogenesis of AS. However, the inhibitor may influence MEK-ERK pathways downstream of receptors other than FGFR2, such as epidermal growth factor receptor (Herbst, 2004) and vascular endothelial growth factor receptor (Ferrara et al., 2003), leading to undesirable effects. In addition, since U0126 only inhibits the MEK-ERK pathway, it would not inhibit other signaling pathways that are downstream of FGFR2. In contrast, all signaling pathways downstream of FGFR2 are possibly affected by sFGFR2IIIc^{S252W} because sFGFR2IIIc^{S252W} functions at the ligand-receptor binding level. As such, sFGFR2IIIc^{S252W} would be more advantageous than U0126 for the potential treatment of AS. On the other hand, sFGFR2^{S252W} would be difficult to use practically in terms of bioavailability and pharmacokinetics, compared to small molecule inhibitors that target FGFR2 signaling. It is difficult to envisage sFGFR2IIIc^{S252W} being delivered in utero to correct developmental defects associated with AS.

To further elucidate the mineralization status of the calvaria in the Apert mouse model, we examined the BMD of the parietal bone of Ap and Ap/Sol mice by quantitative micro-CT analysis. Kreiborg et al. indicated that human Apert calvaria was hypomineralized based on CT examinations (Kreiborg & Cohen, 1990). We did not observe any significant differences in the BMD among wild-type, Ap, and Ap/Sol mice. However, calvaria at P1 may be too small and thin to detect differences in BMD. It is also difficult to configure equal regions of interest (ROIs) because there was considerable variability in the

volume and shape of individual calvaria, particularly in the mutant strains. To evaluate BMD more precisely, we will need an alternative method to micro-CT analysis for future studies.

Our analysis of genotypes of mutant mice indicated that the birth prevalence of *EIIa-Cre*, *sFGFR2IIIc*^{S252W}, *Fgfr2*$^{+/Neo\text{-}S252W}$, *EIIa-Cre sFGFR2IIIc*^{S252W}, and Ap/Sol mice was different from the theoretical ratio. While we do not know the exact mechanism for the difference between the observed prevalence and theoretical ratio, the critical role of FGF signaling during early embryogenesis is apparent.

In conclusion, our study indicates that sFGFR2IIIc^{S252W} can potentially prevent AS-like phenotypes *in vivo*. Some questions remain unanswered, such as determination of the optimum dosage for treatment, an efficacious drug delivery system, and evaluation of other potential side effects.

Experimental Procedures

Generation of the Apert mouse model expressing the soluble form of FGFR2IIIc^{S252W}

Fgfr2$^{+/Neo\text{-}S252W}$, *sFGFR2IIIc*^{S252W}, and *EIIa-Cre* mice have been described previously (Lakso et al., 1996; Chen et al., 2003; Suzuki et al., 2012). *sFGFR2IIIc*^{S252W} mice were first crossed with *EIIa-Cre* mice to generate *EIIa-Cre sFGFR2IIIc*^{S252W} mice. Crossing between male *EIIa-Cre sFGFR2IIIc*^{S252W} mice and female *Fgfr2*$^{+/Neo\text{-}S252W}$ mice generated *EIIa-Cre*, *sFGFR2IIIc*^{S252W}, *Fgfr2*$^{+/Neo\text{-}S252W}$, Ap, *sFGFR2IIIc*^{S252W} *Fgfr2*$^{+/Neo\text{-}S252W}$, *EIIa-Cre sFGFR2IIIc*^{S252W}, and Ap/Sol mice. These mice were bred on a mixed background, and then genotyped by PCR analysis of genomic DNA prepared from tail tips with primers specific

for *Fgfr2*, *Fgfr2*$^{Neo\text{-}S252W}$, *Fgfr2*^{S252W}, *Cre*, and *sFGFR2IIIc*^{S252W}*-3xFLAG*. The primers for *Fgfr2*, *Fgfr2*$^{Neo\text{-}S252W}$, *Fgfr2*^{S252W}, and *sFGFR2IIIc*^{S252W}*-3xFLAG* have been described previously (Holmes et al., 2009; Suzuki et al., 2012) (Fig. 1A, B). The primers for Cre were 5′ -CCTGTTTTGCACGTTCACCG-3′ and 5′ -ATGCTTCTGTCCGTTTGCCG-3′ (290 bp) (Fig. 1B). All experiments were performed in accordance with protocols certified by the Institutional Animal Care and Use Committee of Tokyo Medical and Dental University (#0120272A).

Protein preparation and western blot analysis

Serum was collected from wild-type and *sFGFR2IIIc*^{S252W} mice. FLAG-tagged sFGFR2IIIc^{S252W} protein was purified using a FLAG M Purification Kit (Sigma, St. Louis, MO, USA) according to the manufacturer instructions. Samples were loaded onto a 10% SDS-polyacrylamide gel and transferred to a polyvinylidene difluoride membrane (Amersham Biosciences, Piscataway, NJ, USA). The membrane was incubated with an anti-FLAG antibody (Sigma), and then probed with a horseradish peroxidase-conjugated anti-mouse IgG (Cell Signaling, Danvers, MA, USA). Bound antibodies were detected using an ECL Plus Western Blotting Detection System (Amersham Biosciences) according to the manufacturer's instructions.

μCT imaging protocols of mouse skulls

All mouse samples were scanned at 45 kV, 200 μA, and 12 μm/voxel using a high-resolution X-ray micro-CT system (SMX-100CT; Shimadzu, Kyoto, Japan). BMD, calvaria, and IFS